UCID- 20510

TIBER WINDING PACK DESIGN

John R. Miller

August 19, 1985

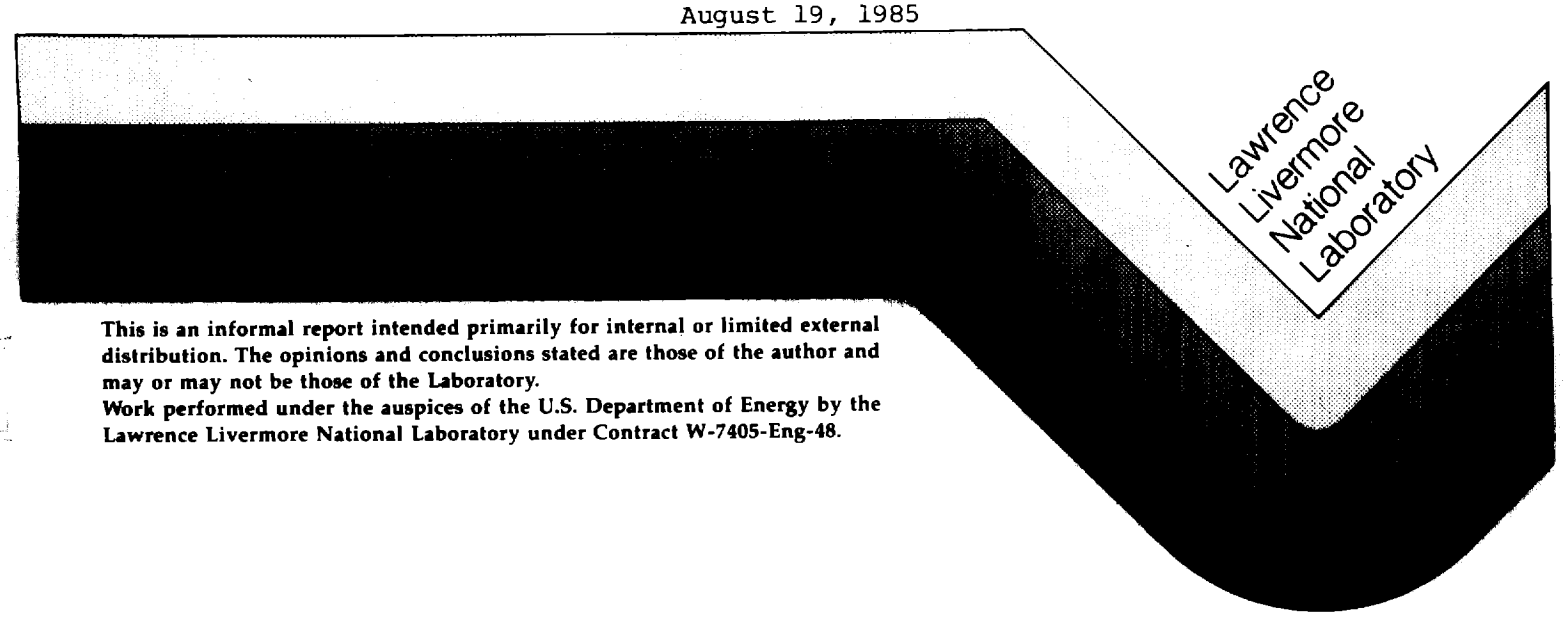

Work performed under the auspices of the U.S. Department of Energy by the Lawrence Livermore National Laboratory under Contract W-7405-Eng-48.

DISCLAIMER

Printed in the United States of America
Available from
National Technical Information Service
U.S. Department of Commerce
5285 Port Royal Road
Springfield, VA 22161
Price: Printed Copy $; Microfiche $4.50

Page Range	Domestic Price	Page Range	Domestic Price
001-025	$ 7.00	326-350	$ 26.50
026-050	8.50	351-375	28.00
051-075	10.00	376-400	29.50
076-100	11.50	401-426	31.00
101-125	13.00	427-450	32.50
126-150	14.50	451-475	34.00
151-175	16.00	476-500	35.50
176-200	17.50	501-525	37.00
201-225	19.00	526-550	38.50
226-250	20.50	551-575	40.00
251-275	22.00	576-600	41.50
276-300	23.50	601-up[1]	
301-325	25.00		

[1]Add 1.50 for each additional 25 page increment, or portion thereof from 601 pages up.

TIBER WINDING PACK DESIGN

Preliminary Work

A preliminary winding pack design was performed with the goal of showing feasibility of producing 10-T maximum field with a pack current density of 40 $A \cdot mm^{-2}$ while accepting 2.7 kW per coil nuclear heating. A cable-in-conduit conductor design (CICC), reported at the 6th Topical Meeting on the Technology of Fusion Energy,[1] was based on several key issues summarized below.

Heat Removal--Local heat transfer was not seen as a critical issue, rather constraining the coolant temperature rise in a conductor flow path to a level consistent with a comfortable level of conductor stability was identified as most important. Simple but conservative formulae were used to select flow path length, injection temperature and pressure of the supercritical helium coolant, pressure drop through a passage, outlet temperature, and temperature rise in an innermost turn. It appeared that double pancakes with two-in-hand winding and helium injection at the inside cross-over would give cooling channels sufficiently short to limit the temperature to a maximum of about 5.6 K at the outlets. Pressure drop was estimated at about 2.4 atm, allowing an inlet pressure in the neighborhood of 5 atm, a range where the heat capacity of helium is very high. More detailed calculations done in conjunction with the refrigeration system design indicated that these preliminary estimates were indeed quite conservative.

Mechanical Loads--Tensile and centering loads on the inner, vertical leg of a TF coil were estimated to examine their impact on winding pack design. The centering force causes a build up of pressure on the outermost turns of a TF coil inner leg (those turns nearest the center of the machine). That pressure was estimated to be about 53 MPa. A CICC with the dimensions and conduit wall thickness of the Westinghouse/Airco LCP conductor has been demonstrated to be capable of sustaining such loads in an impregnated winding.[2] The TIBER conductor therefore was given similar sheath dimensions. Tensile loads were assumed to be shared between the coil case and the steel in sheath of the CICC windings. The estimated stress for the baseline TF coil cross section was modest, 266 MPa. Approximately 62% of the tensile load was born by the case in this configuration, and the remaining 38% by the steel in the CICC windings.

Stability--The fraction of conductor inside the sheath of the CICC and the fraction of copper inside the conductor were optimized for maximum conductor stability subject to the constraints that the fraction of copper not be less than the "manufacturable" limit and that the heat transfer surface provided by the cable strands not fall below the value determined by the "limiting current for multiple stability."[3] It should be remembered that these limits are not rigid

but are prudent for preliminary design.

The stability available with the optimized design was quite high. Calculations were based on data for critical current density vs temperature representative of the Airco bronze process MF-Nb_3Sn conductor developed for the Westinghouse LCP coil (see Fig. 1).[4] The data were degraded to account for compressive prestrain due to differential cooldown stresses developed in a cable inside a steel conduit (the lower curve in Fig. 1). Even assuming the high field turns to be exposed to the outlet temperature of 5.4 K, the ratio of operating current to critical current would be $I/I_c = 0.59$. The current sharing temperature was calculated to be $T_{cs} = 7.4$ K. These figures indicate that some level of stability might be traded for higher winding pack current density.

Current Developments

Time has allowed an iteration of the various preliminary choices of machine parameters. The impact of these choices has been felt on the design of the winding pack. Since it appeared in the first cut that there was indeed margin for change without unduly sacrificing stability, heat removal, or reliability, the design has been reexamined to test just how much change might be accommodated. Also in the meantime, new technological developments have occurred, and clarification of some key constraints placed on the winding pack by other features of the TIBER design has been obtained.

Updated critical current database--Significant advances in MF-Nb_3Sn conductor technology have been obtained by Ti additions to the compound and by fabricating conductors with ultra-fine filaments. Suenaga recently illustrated these advances with the exposition of some of his own measurements (cf. Fig. 2).[5] The solid curves represent conductors with Ti additions and the broken curves, those with pure Nb_3Sn. More detail about the variations responsible for the range of data is not necessary here. It is sufficient to note that all conductors represented in Fig. 2 give higher critical current than the conductor represented in Fig. 1.

The design of a CICC requires more information about the critical current than a single value at a particular field and temperature. Since stability of a CICC is obtained by providing a temperature margin within which heat deposited in the conductor is absorbed by interstitial helium, it is essential to include knowledge of the temperature variation of the critical current in the design process. There is an extensive data base, including temperature dependent data, associated with the conductor represented in Fig. 2 by the emboldened solid curve connecting open diamond data points.[6] Figure 3 displays part of this data base.

It is apparent that, over the temperature range of interest, the

temperature dependence of the critical current at a particular field is essentially linear. Therefore, it can be fully represented by the vertical and horizontal intercepts, $J_{cc}(B)$ and $T_c(B)$ respectively. These intercepts, obtained from the data of Fig. 3 and similar data on identical couductors, are correlated with field variation in Figs. 4 and 5. Figure 5 shows that a linear variation of T_c with B is an adequate representation, but is apparent that values of J_{cc} must be obtained by extrapolation or interpolation from a display like that of Fig. 4. For the present iteration of winding pack design, J_{cc} = 1196 $A \cdot mm^{-2}$ and T_c = 11.89 K have been chosen as representative for the 10 T design maximum field. It should be noted that these values correspond to data from Fig. 2 at the lower edge of the band at 10 T, and as such, represent conservative choices.

Corrections for cooldown strains--The materials inside a CICC all have different coefficients of thermal expansion. As a result, it should not be too surprising that the superconducting Nb_3Sn filaments are put under compression by the action of cooling down from the Nb_3Sn formation temperature (~ 1000 K) to the operation temperature of the magnet. The amount of compression depends on fractions of the various materials and their physical and mechanical properties. It also appears to depend on the compactness of the cable inside the conduit. A correlation of existing data suggests that the filaments of a conductor of the description being proposed for TIBER will experience a compressive strain of about 0.4% due to cooldown.[7]

Ekin has given a formalism for predicting the strain degradation of critical current in Nb_3Sn conductors.[8] For the conductor selected for TIBER, Ekin's predictions are depicted graphically in Fig. 6. The upper curve corresponds to 4.2 K operation and the lower curve to 5.6 K operation. Background field of 10 T is assumed for both. The result of Fig. 6 can alternatively be expressed as a reduction of both J_{cc} and T_c. It is straightforward to show that 0.4% compressive strain yields new values J_{cc} = 1038 $A \cdot mm^{-2}$ and T_c = 11.29 K at 10 T.

Selection of these values for design purposes should be considered as conservative on two counts. First, the turns of conductor in the inner, vertical leg will be subjected to significant tensile load that should reduce the compressive strain caused by cooldown and improve the critical properties at the actual operating conditions.[7] Development is underway that may allow accounting for this improvement by design. Second, Hoenig and his colleagues at MIT have demonstrated that alternate sheath materials can be selected to reduce the cooldown strain.[9] Thus methods are in the offing to provide gains in critical current in a CICC without further development directly on the superconductor, but for now we take account of these developments only as a margin of conservatism.

Stability--The sudden deposition of energy that a CICC can absorb per unit volume of conductor without experiencing an irreversible

quench is referred to as its stability margin ΔH. It has the form[10]

$$\Delta H = S_{He} (T_{cs} - T_b)(A_{He} / A_{cond}) \quad .$$

In the above S_{He} is the effective volumetric heat capacity of the helium between the initial bulk fluid temperature T_b and the current sharing temperature of the conductor T_{cs}. The last factor, the ratio of helium to conductor cross sections, merely refers the absorbed energy to the conductor volume.

The influence of stability on conductor design can be better visualized by casting the above in another form that results from the linear variation of critical current with temperature already discussed:

$$\Delta h = \frac{\Delta H}{S_{He} T_c} = \frac{(1 - f_{cond})}{f_{cond}} \left[\left(\frac{T_c - T_b}{T_c} \right) - \frac{J}{f_{cond} (1 - f_{Cu}) J_{co}} \right] \quad .$$

In this form, the dimensionless stability parameter Δh has the properties of the coolant factored out leaving only the parameters representing the conductor and the operating conditions: f_{cond} is the fraction of conductor inside the conduit (thus, $1 - f_{cond}$ is the fraction left for helium), f_{Cu} is the fraction of copper in the conductor strands, and J is the desired current density over the cable space, i.e. the area inside the conduit.

Contours of the stability parameter are plotted in the (f_{cond}, f_{Cu}) plane in Fig. 7 for the conductor critical parameters already discussed and for T_b = 5.6 K and J = 77.6 $A \cdot mm^{-2}$, which corresponds to J_{pack} = 45 $A \cdot mm^{-2}$ for the present case. It is apparent that for a particular copper fraction in the conductor, there is a unique conductor fraction that gives the highest stability. We do not have complete freedom to choose the configuration giving highest stability; e.g. we have already mentioned a possible "manufacturing" limit on the copper fraction, and there are other limits. It will, however, be convenient to examine the constraints on conductor design in the light of a mapping like Fig. 7 in order that we choose the configuration giving the maximum available stability subject to the constraints.

Effect of end-of-life damage to copper stabilizer--The current shield design for TIBER will allow damage to the copper stabilizer of the conductor in some sections of a TF coil of up to D = 0.009 dpa per

year. This damage will cause and increase in the residual resistivity of the matrix according to the following:[11]

$$\Delta\rho_o = s[1 - \exp(-iD/s)] \quad ,$$

where s is the saturation level and i is the saturation rate. Sawan[12] gives s = 3 nΩ·m and i = 720 nΩ·m·dpa^{-1} while Klabunde, et al.[11] give s = 4 nΩ·m and i = 649 nΩ·m·dpa^{-1}. We use s = 3.46 nΩ·m and i = 696 nΩ·m·dpa^{-1} as a compromise. Note that for the anticipated damage only the saturation level and not the rate is important.
Magnetoresistivity is accounted for by the relation

$$\rho(B) = \rho_o[1 + 0.0339(B/\rho_o)^{1.07}] \quad ,$$

where ρ_o includes the effects of radiation damage.[13]

For a CICC design the copper resistivity does not to first order affect the stability level provided.[14] It does influence the amount of conductor surface required to effectively utilize the heat capacity of the interstitial helium as can be seen by the variation of the "limiting" current for multiple stability J_{lim} with $\rho^{-1/2}$. The requirement for better heat transfer as copper damage accumulates may already be provided by the high flow rates required for steady state heat removal, however. A more important requirement will be that of protection as the coils approach end-of-life.

Limiting current--The limiting current density in a CICC is the value below which full stability is available even with initially stagnant helium inside. As such it may be viewed as a good indicator that heat transfer from the cable to the helium is good enough even without being augmented by net flow. It is prudent initially to choose a conductor configuration for which the limiting current density J_{lim} exceeds the design value for the cable space current density J. Towards the end-of-life as copper damage accumulates to reduce J_{lim}, the loss will be offset by the flow already required for heat removal. In Fig. 8, the contours of the stability parameter have been overlaid with contours of $J_{lim} = J$ for both initial and end-of-life residual resistivity. The current design will observe the constraints on conductor configuration due to the former and ignore those due to the latter.

Protection--There two areas that must be examined to evaluate whether protection is adequate for a coil using a CICC: maximum pressure inside the conduit in the event of a quench and maximum hot-spot temperature in the event of a quench. The former depends strongly on distance between flow connections.[15] That distance will be short in the TIBER design to facilitate heat removal; pressure rise

should not be too great a problem. However, a full evaluation must await further tuning of the design. The latter can be addressed now.

The upper limit to the cable space current density in terms of the allowed maximum hot-spot temperature can be determined from the following expression:

$$J \le \sqrt{(2/\tau)} \left[(1 - f_{cond}) f_{cond} f_{Cu} \int_{T_b}^{T_{max}} \frac{\mu_{He,init}\, c_{v,He}}{\rho_{Cu}}\, dT \right.$$

$$+ f_{Cu}^2 f_{cond}^2 \int_{T_b}^{T_{max}} \frac{\mu_{Cu}\, c_{Cu}}{\rho_{Cu}}\, dT$$

$$\left. + (1 - f_{Cu}) f_{Cu}^2 f_{cond} \int_{T_b}^{T_{max}} \frac{\mu_{n.c.}\, c_{n.c.}}{\rho_{Cu}}\, dT \right]^{1/2},$$

where μ_i and c_i are the density and heat capacity, respectively, of the various materials and ρ_{Cu} is the electrical resistivity of the copper in the conductor. The dump time constant τ is given simply by

$$\tau = (2 E_s / V_d I_{op}) \quad ,$$

where E_s is the stored energy per TF coil, V_d is the dump voltage across the terminals of an individual coil, and I_{op} is the operating current. Experiments simulating a fully quenched CICC have shown that the conductor temperature rise is consistent with the assumption that the initial density of the helium and the constant volume heat capacity of the helium (essentially constant and approximately equal to 3.1 $kJ \cdot kg^{-1} \cdot K^{-1}$) are the appropriate choices for the values in the first term of the above equation (as indicated).[15]

Figure 9 shows contours of J equal to the protection limit, calculated with the end-of-life resistivity in the copper. Both contours were calculated with T_{max} = 100 K, but the upper was calculated with V_d = 5 kV and the lower was calculated with V_d = 10 kV. It should be noted that essentially the same constraints on conductor parameters as given by the (T_{max}, V_d) = (100 K, 10 kV) limits are obtained with (200 K, 5 kV) or (300 K, 3 kV). All three of these contours are shown on the same mapping in Fig. 10.

It is more or less a matter of philosophy and a question of into which area to put the most development effort as to which contour in Fig. 10 is seen as the most reasonable constraint. However, there is in fact little difference between them, and the moral to the story

here is that protection of the TF coils at end-of-life is looms as the most severe constraint to pushing the winding pack current density much above 45 $A \cdot mm^{-2}$, because void fraction of around 40 % is needed to facilitate heat removal and to lessen the effect of compressive prestrain on the superconductor, conductors with copper fraction less than about 60 % may be difficult to manufacture, and stability corresponding to a stability parameter of 0.1 or greater is highly desirable. For these reasons we select a winding pack current density of 45 $A \cdot mm^{-2}$, which will be achieved with a CICC having $f_{sc,ns} = 0.6$ and $f_{Cu} = 0.6$.

Summary

Tables I and II summarize the coil and winding pack parameters, respectively. Figure 11 shows the winding pack configuration consistent with Tables I and II, and Fig. 12 shows a unit cell of the winding.

Table I. TF COIL PARAMETERS

NI	65 MAT
N_{coils}	16
B_T	5.0 T
R_p	2.6 m
R_1	1.06 m
R_2	1.30 m
R_1'	1.02 m
R_2'	1.33 m
$\langle R_1 \rangle$	1.17 m
$\langle R_o \rangle$	4.5 m
h	2.5 m
$\langle L \rangle$	13.7 m
B_{max}	10.0 T
E_s	150 MJ
V_d	5.0 kV
I_{op}	21 kA

Table II. COIL PACK PARAMETERS

Coil X-section (straight leg)	0.143 m^2
Winding pack X-section	0.0903 m^2
N_{turns}	192
J_{pack}	45 $A \cdot mm^{-2}$
A_{eff}	$(21.67\ mm)^2$
J	77.6 $A \cdot mm^{-2}$

Overall materials fractions:

f'_{steel}	0.25
f'_{insul}	0.17
f'_{cond}	0.35
f'_{He}	0.23

Materials fractions in the CICC:

f_{cond}	0.60
f_{He}	0.39
f_{Cu}	0.60

REFERENCES

1. C.D. Henning, "TIBER - A SUPERCONDUCTING TOKOMAK IGNITION DEVICE,"presented at the 6th Topical Meeting on the Technology of Fusion Energy, San Francisco, CA, March 3-7, 1985.

2. H. Becker, et al., "Structural behavior of Internally Cooled Cabled Superconductors under transvers load," PFC/RR85-10, internal report of the MIT Plasma Fusion Center, June 1985

3. J.R. Miller and J.W. Lue, Stability of Superconductors in HeI and HeII, Proceedings of the Workshop held at Saclay (France), (International Institute of Refrigeration, Paris, France, 1981), p. 247.

4. P.A. Sanger, et al., IEEE Trans. Magn. MAG-17 (1981) 666.

5. M. Suenaga, "Workshop on Conductor-Sheath Issues for ICCS," July 1985.

6. M. Suenaga, et al., Cryogenics 25 (1985) 123.

7. J.R. Miller, "Workshop on Conductor-Sheath Issues for ICCS," U.S. Department of Energy - Germantown, July 15-16, 1985.

8. J.W. Ekin, Cryogenics 20 (1980) 611.

9. M.M. Steeves and M.O. Hoenig, IEEE Trans. Magn. MAG-19 (1983) 374.

10. J.R. Miller, "Design of Aggressive Superconducting TFCX Magnet Systems," presented at 6th Topical Meeting on the Technology of Fusion Energy, San Francisco, CA, March 3-7, 1985.

11. C.E. Klabunde, et al., Journal of Nuclear Materials, 85 & 86 (1979) 385.

12. M.E. Sawan, "Review of Radiation Effects in Superconducting Magnets and Proposed Radiation Limits," presented at the Workshop on Radiation Limits to Superconducting Magnets, Fusion Technology Institute, University of Wisconsin, May 23, 1985.

13. M.W. Guinan, "Radiation effects limits on copper in superconducting magnets," internal LLNL report UCID-19800, (equation obtained from a fit to data of Fig 3.4.3, "Kohler plot for unoxidized OFHC copper.").

14. J.R. Miller, "Empirical Investigation of factors affecting the stability of cable-in-conduit superconductors," submitted for publication to Cryogenics, May 1985, internal LLNL report UCRL-92551.

15. J.R. Miller, et al., in Proc. 8th Intern. Cryogenic Engineering Conference, (IPC Science and Technology Press, Ltd., Guilford, Surrey, UK, 1980), p. 321.

FIGURE CAPTIONS

Fig. 1 Critical current density over the non-copper fraction for single strands of the MF-Nb_3Sn conductor developed for the Westinghouse LCP coil. The solid line below the one connecting the data points represents a conservative accounting for the compressive strain imposed on the conductor by being reacted and cooled down to operating temperature inside a steel sheath.

Fig. 2 Recent data showing the improvements in MF-Nb_3Sn conductor technology. The solid curves represent conductors with Ti additions to the compound, and the broken curves represent improvements obtained by geometrical changes in the starting billet, i.e. smaller filaments, more Nb, etc. The highlighted solid curve with open diamond points is from the same data base as Fig. 3.

Fig. 3 Critical current density over the non-copper fraction vs temperature at various fields for a Ti modified MF-Nb_3Sn conductor. The data represented here is from the same data base as that represented by the highlighted solid curve in Fig. 2.

Fig. 4 A Kramer correlation of the extrapolated, zero temperature, critical current density values vs field from the reference conductor data base.

Fig. 5 A linear correlation of the extrapolated, zero current, critical temperature values vs field from the reference conductor data base.

Fig. 6 Fraction of the maximum available (unstrained) critical current vs intrinsic filament strain for the reference conductor at 10 T and at 4.2 K and 5.6 K.

Fig. 7 Contours of the stability parameter in the (f_{cond},f_{Cu}) plane with J_{co} = 1038 $A \cdot mm^{-2}$, T_c = 11.29 K, T_b = 5.6 K, and J = 77.6 $A \cdot mm^{-2}$.

Fig. 8 Contours of J_{lim} = J superimposed on the mapping of the stability parameter from Fig. 7. Curve (a) assumes copper with RRR = 100 at 10 T and no damage. Curve (b) assumes 0.009 dpa/year for three years.

Fig. 9 Contours of J at a protection limit superimposed on the mapping of the stability parameter from Fig. 7. Both curves assume copper resistivity at end-of-life damage level and a maximum allowable hot-spot temperature of 100 K. Curve (a) assumes a maximum allowable dump voltage of 10 kV, and curve

(b) 5 kV.

Fig. 10 Similar contours of J at the protection limit superimposed on the mapping of the stability parameter from Fig. 7. Each assumes copper resistivity at end-of-life damage level but different choices of (T_{max}, V_d): curve (a), (100 K, 10 kV); curve (b), (200 K, 5 kV); and curve (c), (300 K, 3 kV).

Fig. 11 A schematic picture of the coil cross section at the midplane of the inner vertical leg. Open squares represent turns of the winding pack in the present configuration. Squares covered over by the cross hatching of the coil case represent deleted turns that were present in the preliminary design with a winding pack current density of 40 $A \cdot mm^{-2}$.

Fig. 12 Representation of a unit cell of the winding pack. The steel jacketed CICC is surrounded by insulation. Dimensions are in mm.

Fig. 1 Critical current density over the non-copper fraction for single strands of the MF-Nb_3Sn conductor developed for the Westinghouse LCP coil. The solid line below the one connecting the data points represents a conservative accounting for the compressive strain imposed on the conductor by being reacted and cooled down to operating temperature inside a steel sheath.

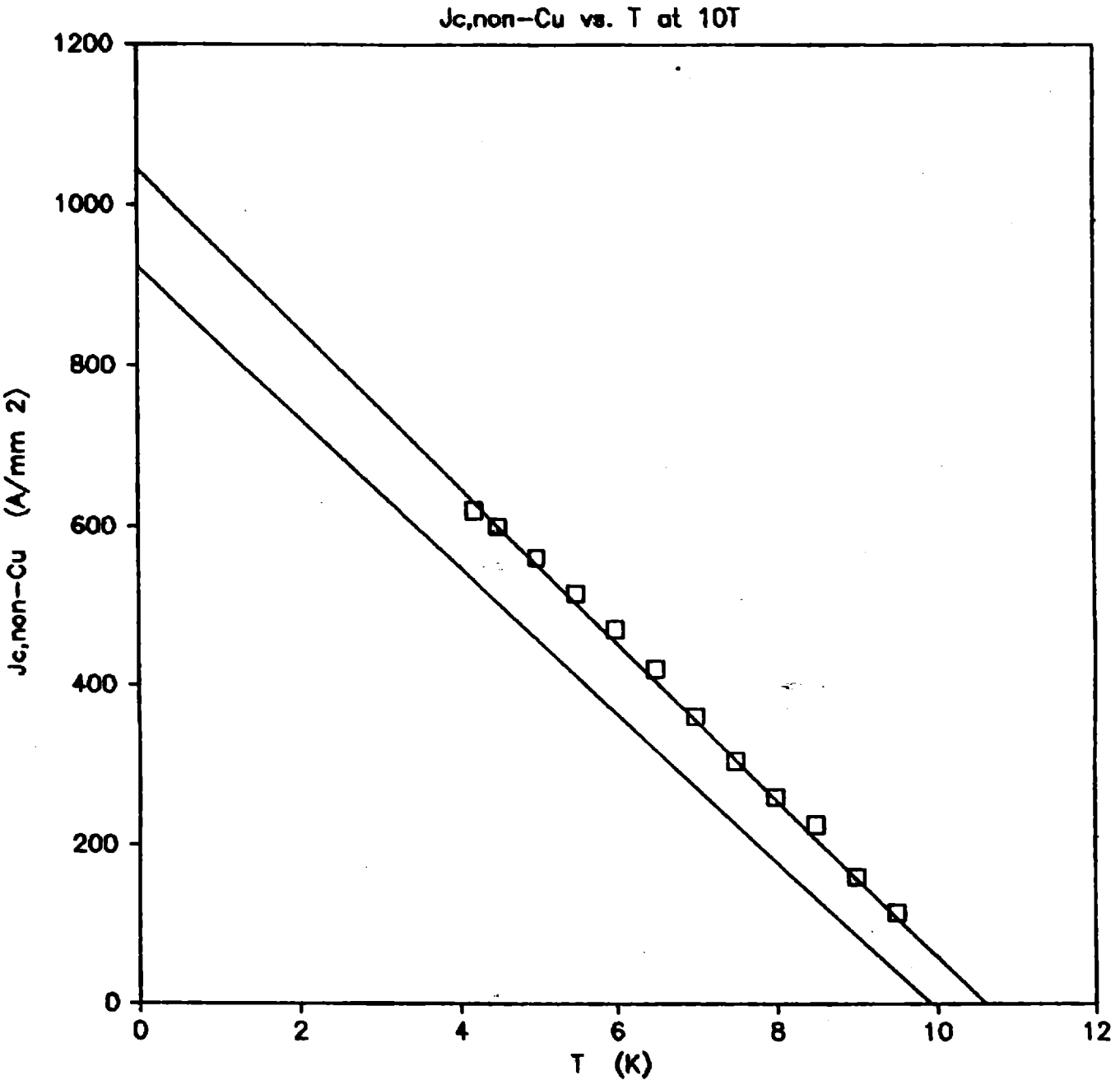

Fig. 2 Recent data showing the improvements in MF-Nb_3Sn conductor technology. The solid curves represent conductors with Ti additions to the compound, and the broken curves represent improvements obtained by geometrical changes in the starting billet, i.e. smaller filaments, more Nb, etc. The highlighted solid curve with open diamond points is from the same data base as Fig. 3.

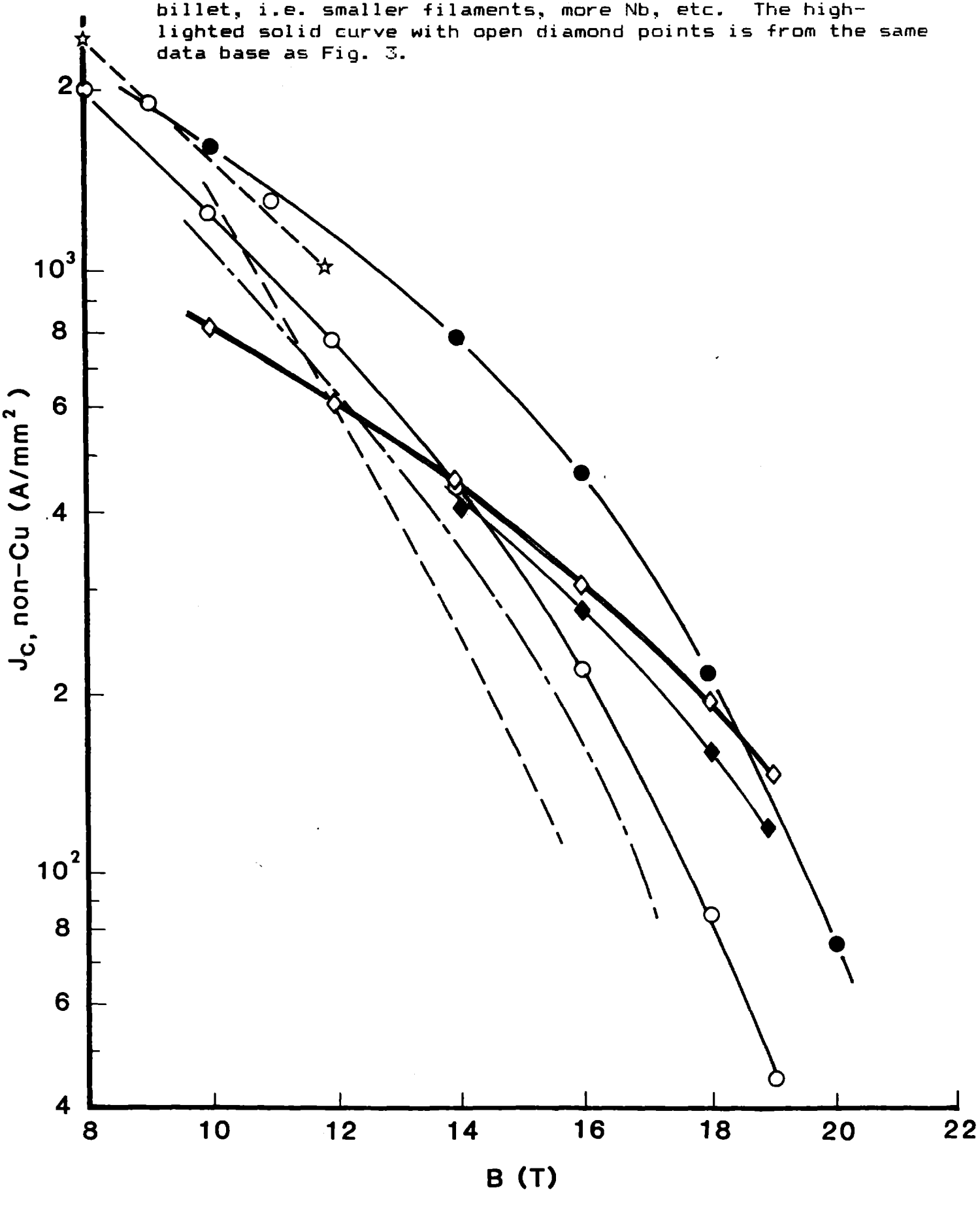

Fig. 3 Critical current density over the non-copper fraction vs temperature at various fields for a Ti modified MF-Nb_3Sn conductor. The data represented here is from the same data base as that represented by the highlighted solid curve in Fig. 2.

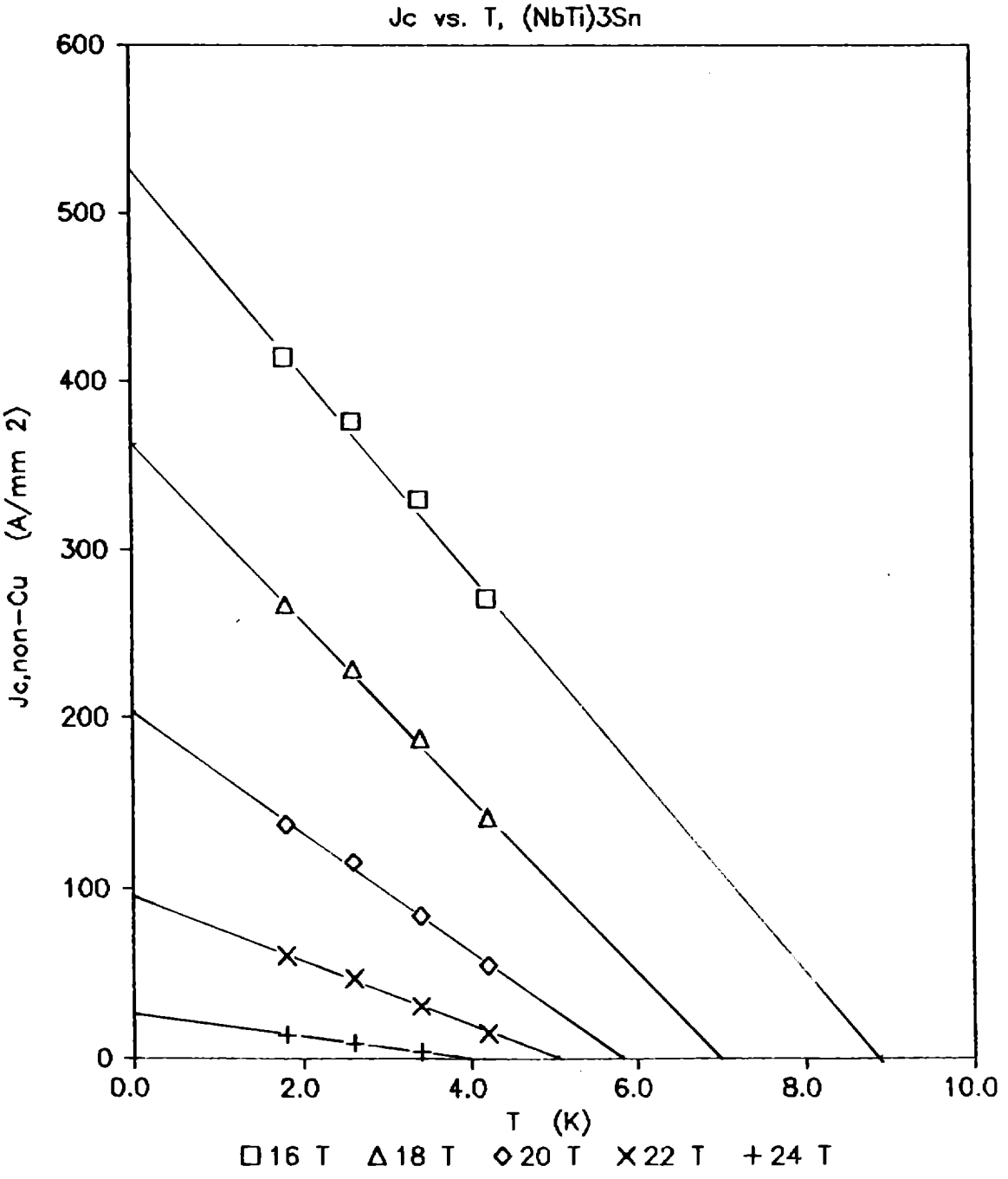

Fig. 4 A Kramer correlation of the extrapolated, zero temperature, critical current density values vs field from the reference conductor data base.

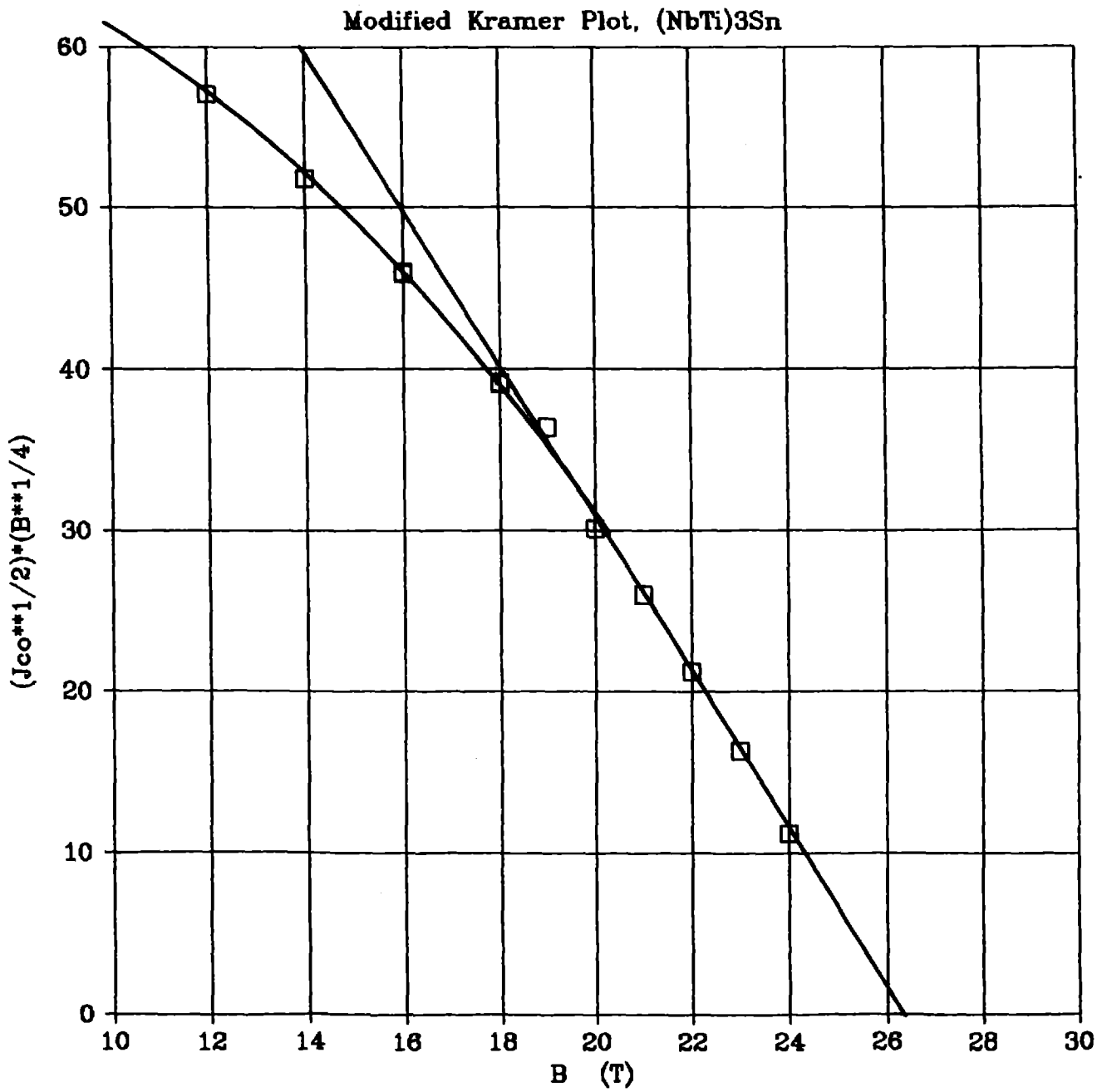

Fig. 5 A linear correlation of the extrapolated, zero current, critical temperature values vs field from the reference conductor data base.

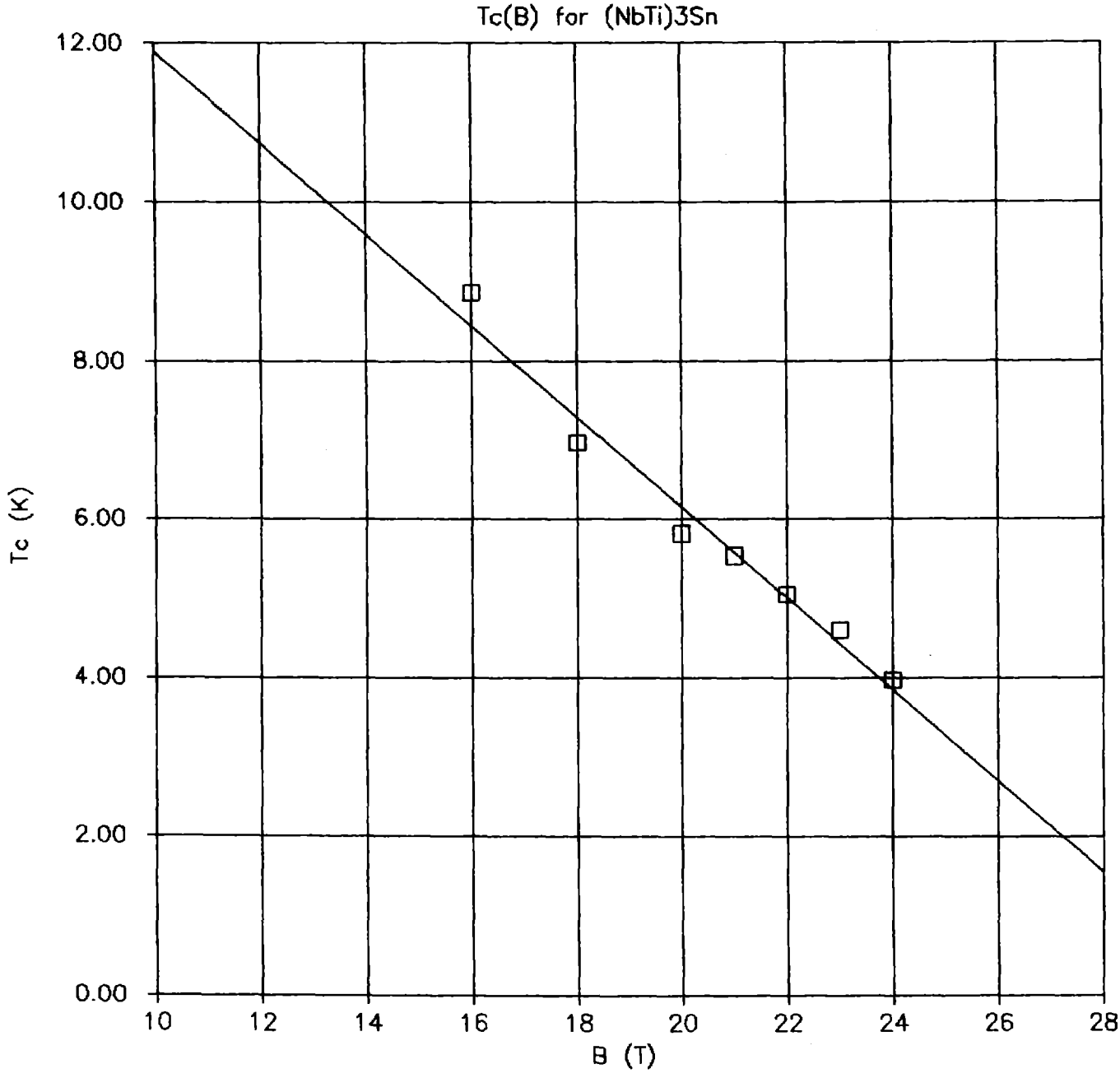

Fig. 6 Fraction of the maximum available (unstrained) critical current vs intrinsic filament strain for the reference conductor at 10 T and at 4.2 K and 5.6 K.

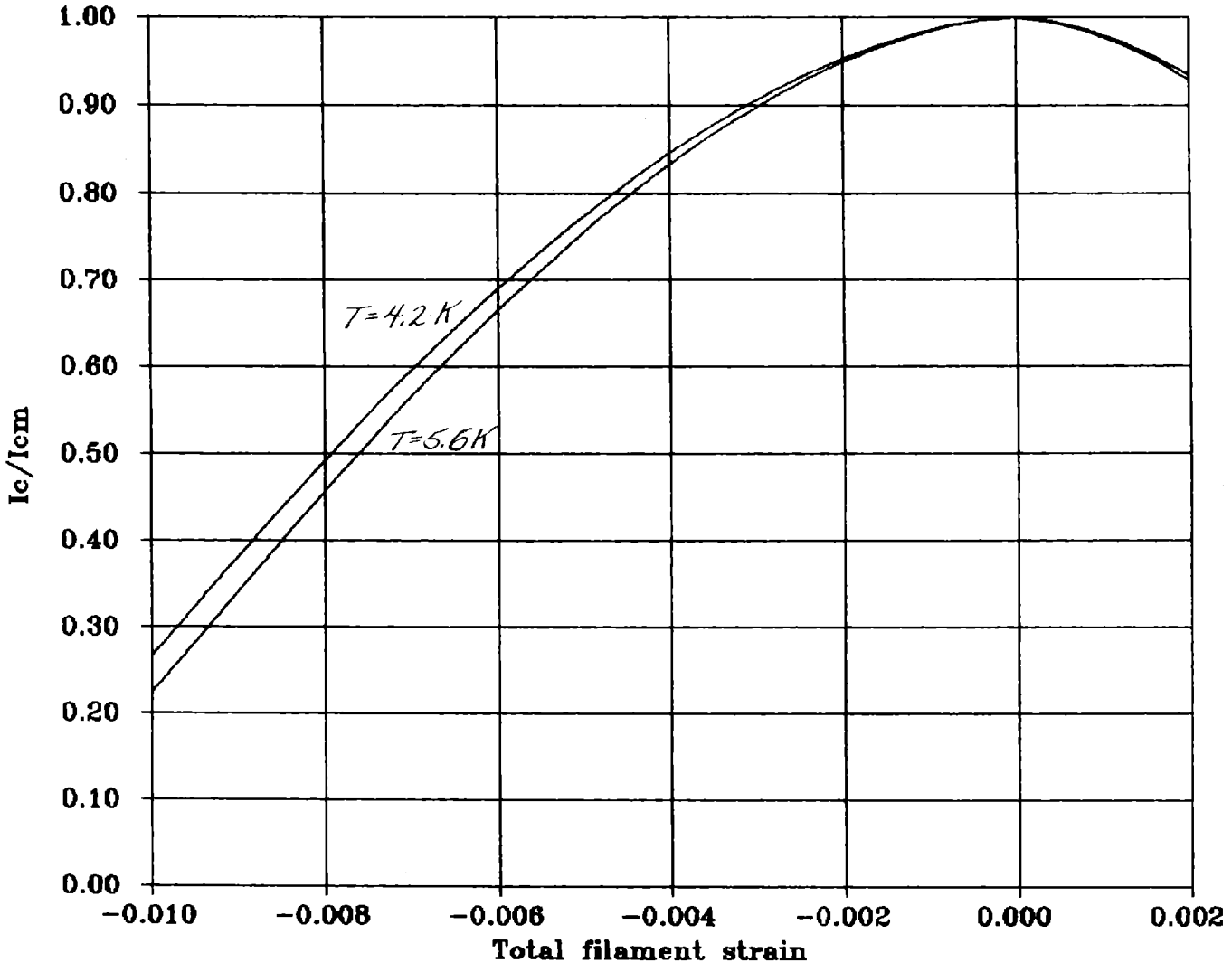

Fig. 7 Contours of the stability parameter in the (f_{cond}, f_{Cu}) plane with J_{cs} = 1038 A·mm^{-2}, T_c = 11.29 K, T_b = 5.6 K, and J = 77.6 A·mm^{-2}.

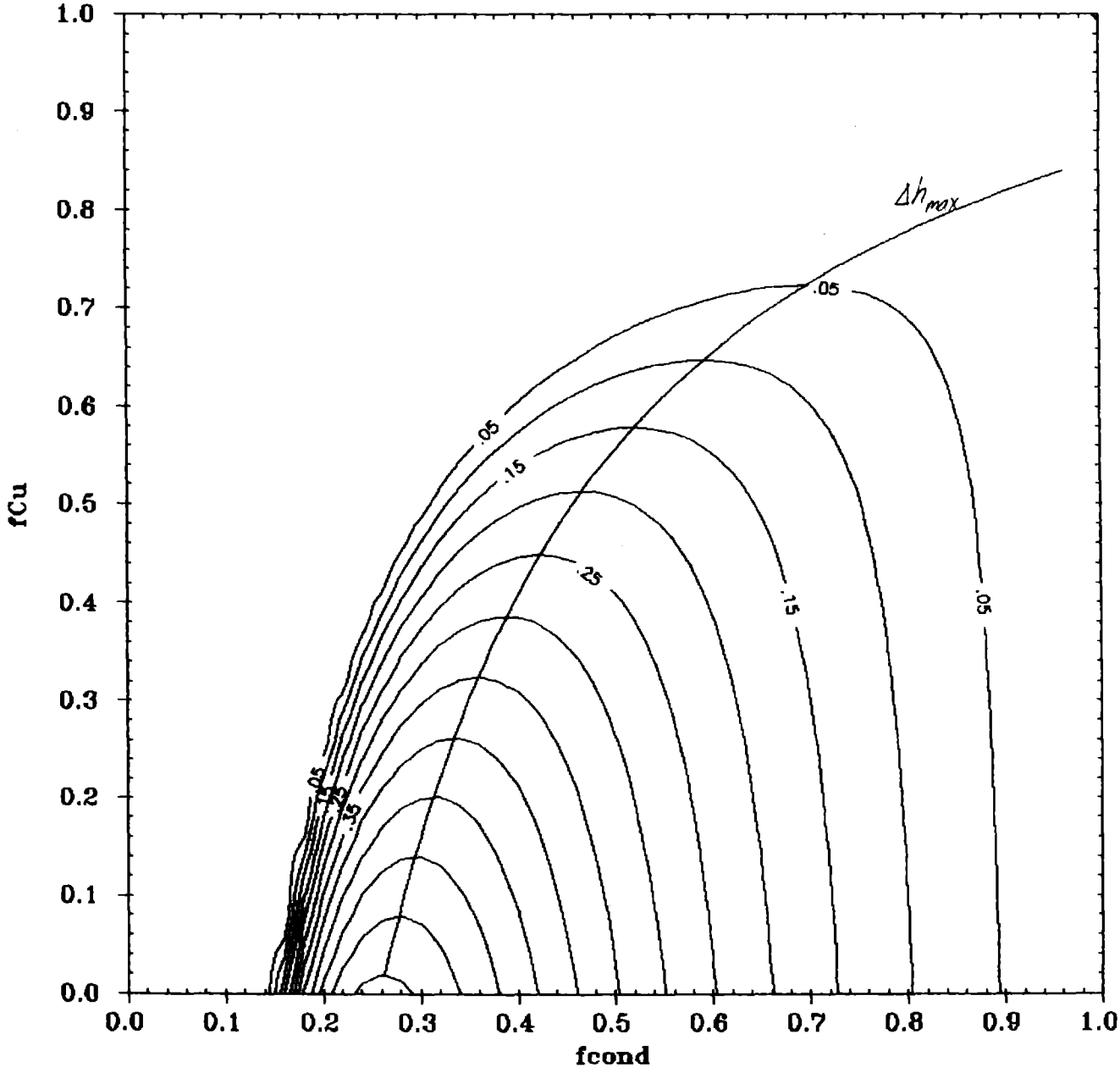

Fig. 8 Contours of J_{lim} = J superimposed on the mapping of the stability parameter from Fig. 7. Curve (a) assumes copper with RRR = 100 at 10 T and no damage. Curve (b) assumes 0.009 dpa/year for three years.

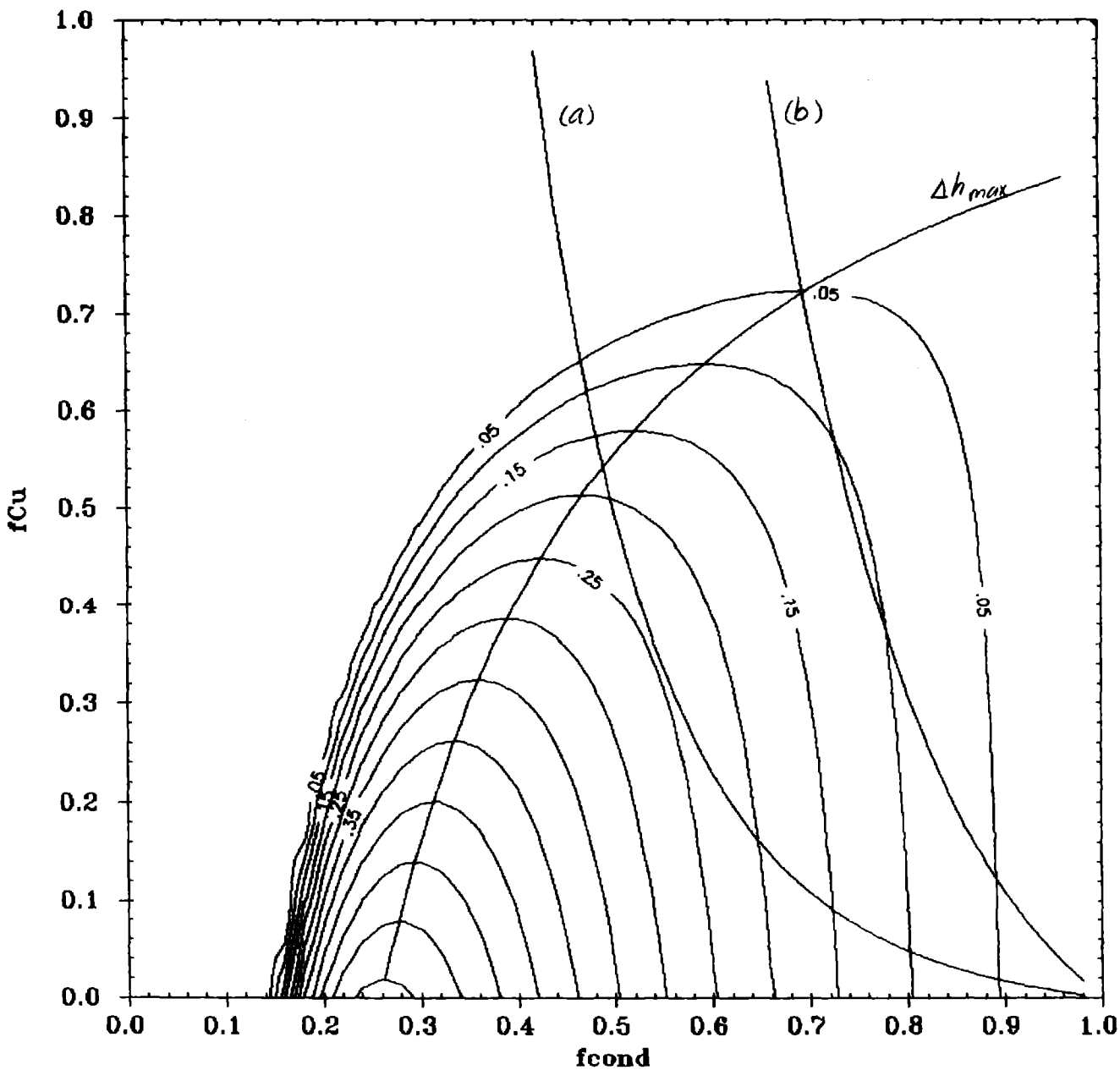

Fig. 9 Contours of J at a protection limit superimposed on the mapping of the stability parameter from Fig. 7. Both curves assume copper resistivity at end-of-life damage level and a maximum allowable hot-spot temperature of 100 K. Curve (a) assumes a maximum allowable dump voltage of 10 kV, and curve (b) 5 kV.

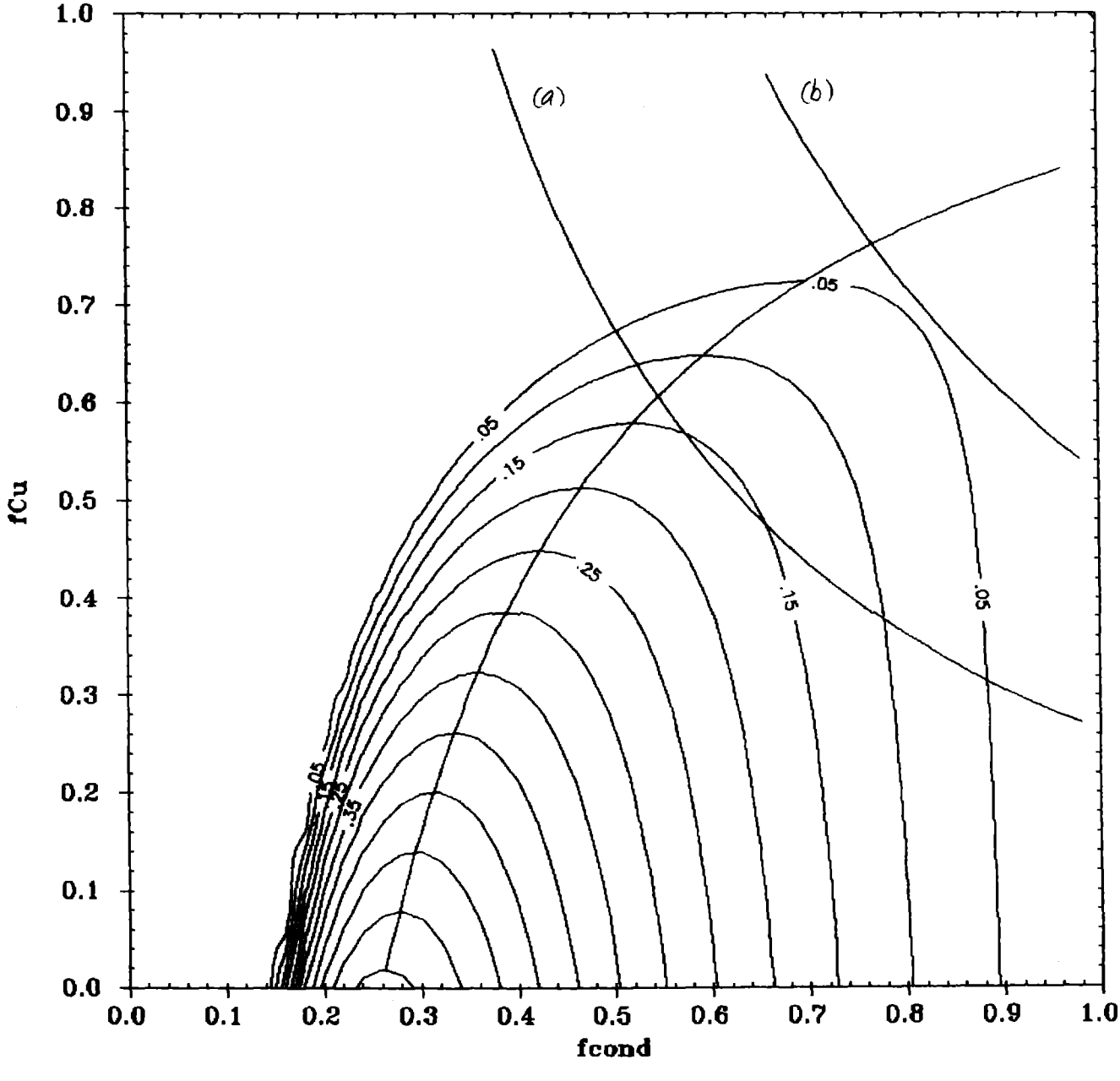

Fig. 10 Similar contours of J at the protection limit superimposed on the mapping of the stability parameter from Fig. 7. Each assumes copper resistivity at end-of-life damage level but different choices of (T_{max},V_d): curve (a), (100 K, 10 kV); curve (b), (200 K, 5 kV); and curve (c), (300 K, 3 kV).

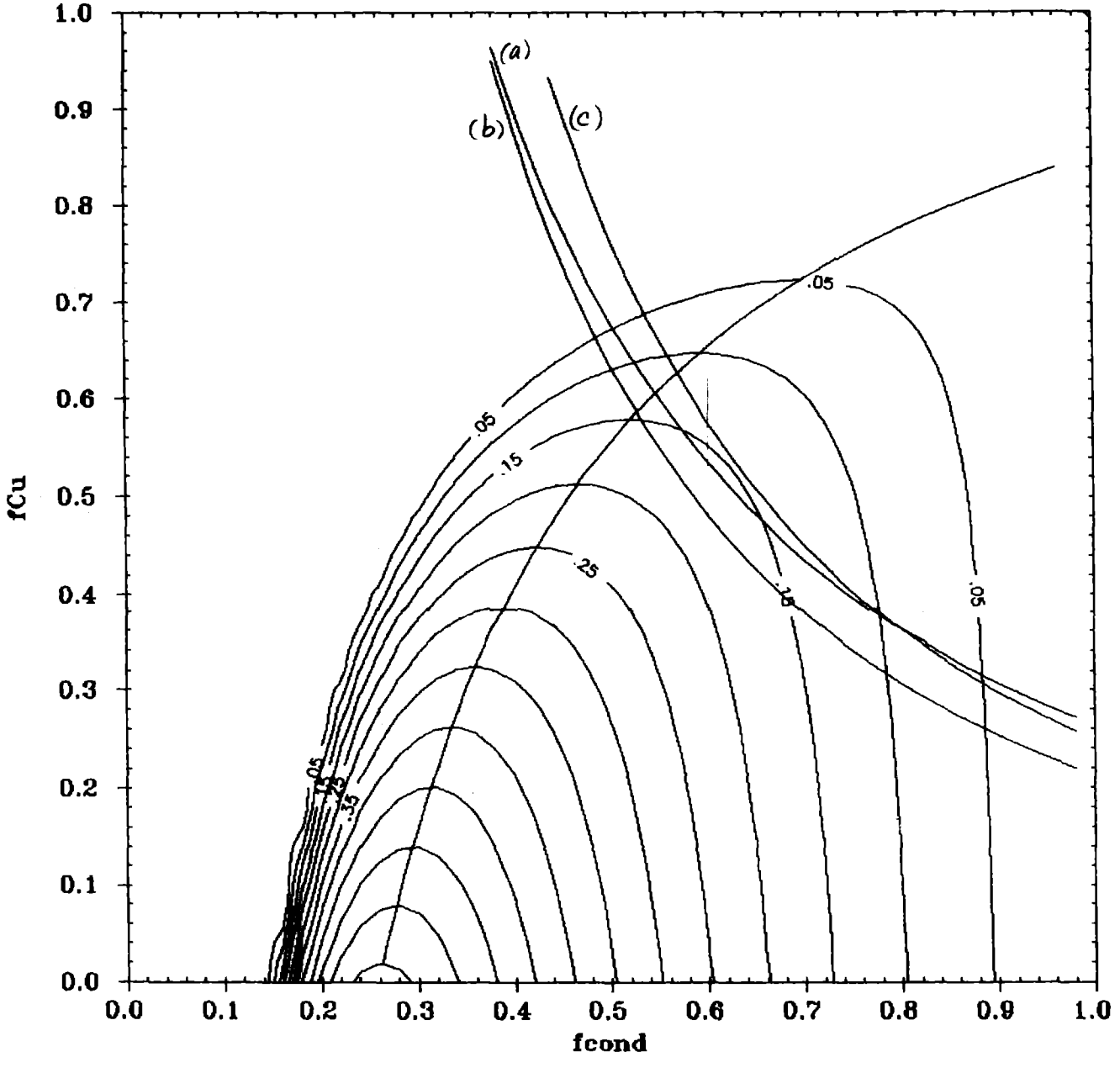

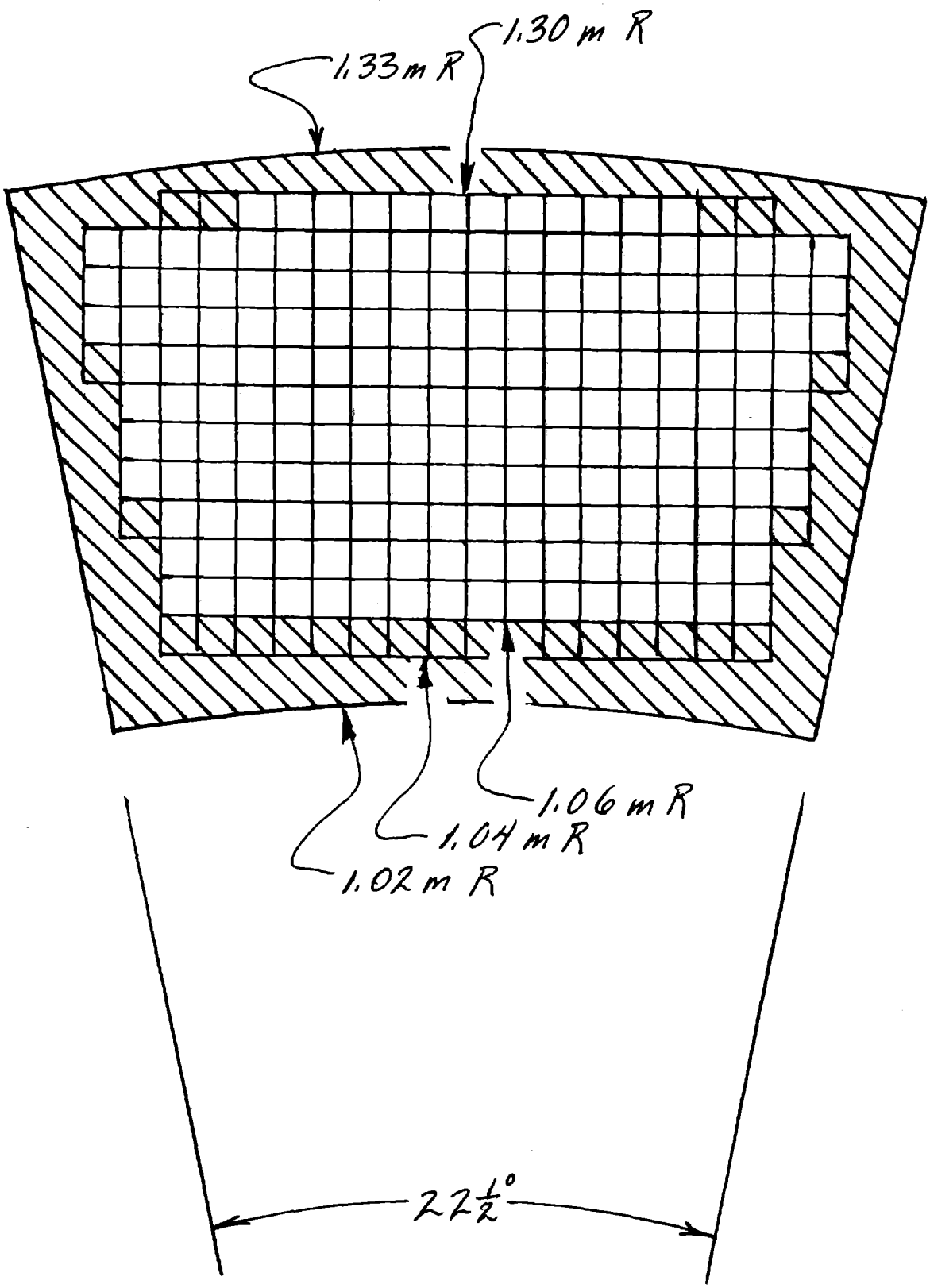

Fig. 11 A schematic picture of the coil cross section at the midplane of the inner vertical leg. Open squares represent turns of the winding pack in the present configuration. Squares covered over by the cross hatching of the coil case represent deleted turns that were present in the preliminary design with a winding pack current density of 40 $A \cdot mm^{-2}$.

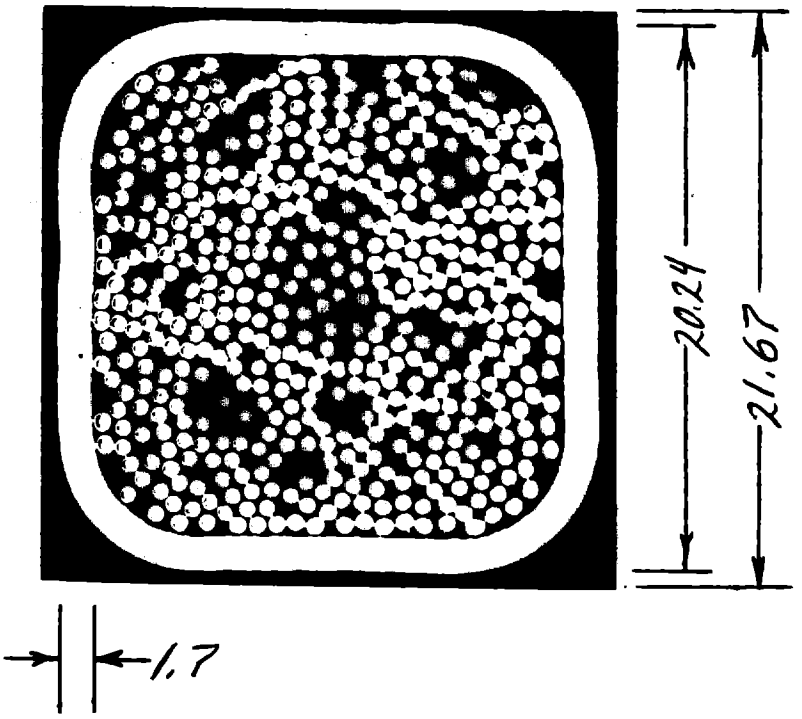

Fig. 12 Representation of a unit cell of the winding pack. The steel jacketed CICC is surrounded by insulation. Dimensions are in mm.